

# REPEAT-PASS SAR INTERFEROMETRY WITH PARTIALLY COHERENT TARGETS

D. Perissin<sup>(1)</sup>, A. Ferretti<sup>(2)</sup>, R. Piantanida<sup>(1)</sup>, D. Piccagli<sup>(1)</sup>, C. Prati<sup>(1)</sup>, F. Rocca<sup>(1)</sup>, A. Rucci<sup>(1)</sup>, F. de Zan<sup>(1)</sup>

<sup>(1)</sup> Politecnico di Milano, Via Ponzio 34/5 20133 Milano Italy, Email: daniele.perissin@polimi.it

<sup>(2)</sup> Tele-Rilevamento Europa – T.R.E. srl – Via Vittoria Colonna 7, 20149 Milano, Italy

## ABSTRACT

By means of the Permanent Scatterers (PS) technique, repeated spaceborne SAR images with slight low resolution (about 25m x 5m for ESA ERS and Envisat) can be used to estimate displacement (1mm precision) and 3D location (1m precision) of targets that show an unchanged electromagnetic signature. The main drawback of the PS technique is the limited spatial density of targets that behave coherently during the whole observation span (hundreds of PS per squared km in urban site, up to few points in vegetated areas). In this work we describe different solutions for multi-temporal analysis of SAR images that allow to extract information also from partially coherent targets. The core idea is to relax the restrictive conditions imposed by the PS technique. The results obtained in different test-sites allowed to increase significantly the spatial coverage of the estimate of height and deformation trend, especially in extra-urban areas.

## 1. INTRODUCTION

SAR Interferometry [1] is a remote sensing technique able to recover high-resolution topographic profiles (precision ~10m) and to highlight possible ground deformation phenomena (precision ~10mm). Topography and movement are extracted from interferograms, complex products of two scenes gathered at different times with different looking angles over the same area of interest. The main limitations of InSAR are temporal and geometrical decorrelation, caused by the variation of the ground reflectivity as a function of the acquisition time and incidence angle. Moreover, interferograms are affected by turbulences related to the spatially variant water vapour content in the atmosphere.

The Permanent Scatterers (PS) Technique [2], developed at POLIMI in late nineties, is a powerful tool in the context of InSAR. By looking at radar targets that maintain unchanged their electromagnetic signature during the whole observation span, the PS technique allows to solve the classical problems of interferometry. The technique has been successfully applied to different cases, from ground deformation monitoring [3] to building stability analysis [4], and also to recover digital elevation maps (DEM) [5]. The accuracy achievable by means of the PS technique is in the order of 1m in the estimate of the target height and 1mm in the estimate of

the target displacement [6]. The main drawback of the PS approach is the low spatial density of permanent targets, in particular in extra-urban areas. Indeed the lack of measure points can prevent from monitoring with spaceborne SAR techniques an area of interest affected by deformations. In this work we present a new approach that relax the strict conditions imposed by the PS technique in order to extract information also from partially coherent targets and thus to increase the spatial distribution of measure points. In particular, three main modifications have been introduced:

1. the images of the data-set are no more required to interfere with a unique common Master image as in the PS technique;
2. in the estimate of the target height and displacement only an appropriate sub-set of interferograms is evaluated;
3. considering extended targets a spatial filtering is applied to enhance the signal to noise ratio of the interferometric phase.

The new approach was successfully applied to the cases of Dossena, a small municipality located in a mountainous area in the Italian province of Bergamo, and of Gardanne, a town and commune of the Bouches-du-Rhône département in southern France. In the following we analyse in depth the main steps of the innovative algorithm.

## 2. ALGORITHM

Let us denote with  $s_i$  the  $i$ -th complex SAR image (with  $i = 1 \dots N$ ). The interferogram between the images  $i$  and  $j$  can thus be expressed as  $I_{i,j} = s_i \cdot s_j^*$ . Taking the target  $p_0$  as reference point, the interferometric phase of target  $p$   $\Delta\phi^{i,j} = \angle I_{i,j}$  depends on its geometrical location as well as on its displacement, atmospheric disturbances and noise. In particular the terms that depend on the target  $p$  height  $\Delta h_{p,p_0}$  and linear deformation trend  $\Delta v_{p,p_0}$  are expressed respectively by:

$$\Delta\phi_{H,p,p_0}^{i,j} = \frac{4\pi}{\lambda} \frac{1}{R \sin \theta} \Delta h_{p,p_0} B n_{i,j} \quad (1)$$

and

$$\Delta\phi_{D,p,p_0}^{i,j} = \frac{4\pi}{\lambda} \Delta v_{p,p_0} B t_{i,j} \quad (2)$$

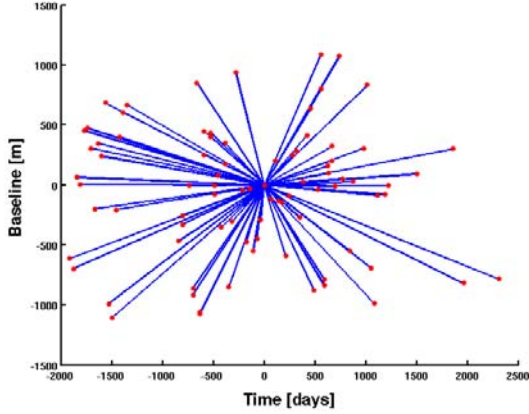


Figure 1. Images graph adopted in the PS technique.

where  $Bn_{ij}$  is the interferometric normal baseline,  $Bt_{ij}$  the temporal baseline,  $\lambda$  the wavelength,  $\theta$  the looking angle and  $R$  the sensor-target distance. Within the PS technique, the target height and velocity are estimated by maximizing  $\xi_p$  [2] (we omit index  $p_0$  to lighten the notation):

$$(\Delta\hat{h}_p, \Delta\hat{v}_p) = \arg\left\{\max\left(|\xi_p|\right)\right\} \quad (3)$$

where

$$\xi_p = \frac{\sum_{i=1}^N e^{j(\Delta\phi_p^{i,j} - \Delta\bar{\phi}_{H,p}^{i,j} - \Delta\bar{\phi}_{D,p}^{i,j})}}{N} \quad (4)$$

In Eq. 4 the following terms can be highlighted:

- $\Delta\phi_p^{i,j}$  is the acquired interferometric phase (compensated for the terms that do not depend on elevation and linear deformation trend);
- $\Delta\bar{\phi}_{H,p}^{i,j}$  is the elevation-dependent term given by Eq. 1;
- $\Delta\bar{\phi}_{D,p}^{i,j}$  is the deformation trend-dependent term given by Eq. 2.

In the classical PS analysis the interferometric phase in Eq. 4 is generated by referring all images to a common Master acquisition. In the normal baseline – temporal baseline space this configuration can be represented with a star graph as in Fig. 1, where each point indicates an image and each connection an interferogram in the Dossena data-set.

In this framework, the graph connection assures the temporal continuity of the deformation measurements and thus the possibility of unwrapping the phase time

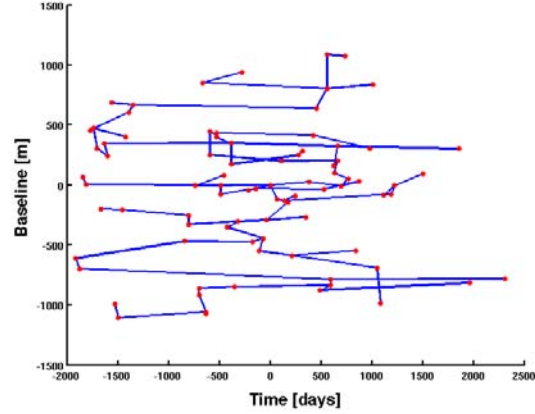


Figure 2. MST obtained by maximizing the average coherence.

series. On the other side, the main drawback of this combination is to pretend that each image can coherently interfere with the Master acquisition. Other less restrictive configurations are also possible (see SBAS [7] or StamPS [8]). The first methodology we propose here is to search for the minimum best coherent graph connecting all the images of the data-set (usually known as the Minimum Spanning Tree, MST [9]), without imposing any pre-defined decorrelation model. To reach this purpose with a limited computational cost, we assign to each graph connection  $i,j$  the absolute value of the spatial coherence  $\gamma_p^{i,j}$  averaged over a set of given points. Then we search among the  $N(N-1)/2$  possible interferograms for the MST that maximizes the average coherence. The spatial coherence  $\gamma_p^{i,j}$  of point  $p$  is retrieved as the normalized cross-correlation coefficient between images  $i,j$  over an appropriate neighbourhood  $Win(p)$  of  $p$ :

$$\gamma_p^{i,j} = \frac{\sum_{Win(p)} S_i S_j^*}{\sqrt{\sum_{Win(p)} |S_i|^2 \sum_{Win(p)} |S_j|^2}} \quad (5)$$

Fig. 2 shows the obtained graph in the Dossena data-set. As visible in the picture, many selected connections have small normal baselines, but not all interferograms follow this rule. Moreover, the graph is connected.

The configuration in Fig. 2 is thus on average the minimum best way to combine the available images. Whenever the baseline statistics of the MST is not sufficient, we can improve it by adding conveniently more connections, in spite of a limited growth of computational costs. E.g. by doubling the number of graph connections (selecting the most coherent interferograms not yet used) we obtain the graph shown in Fig. 3.

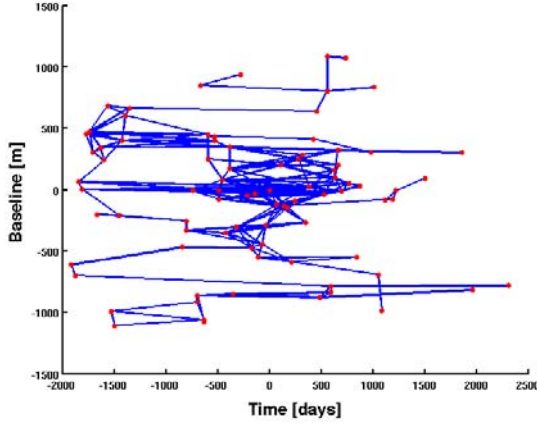


Figure 3. Images graph obtained doubling the number of connections with respect to the MST.

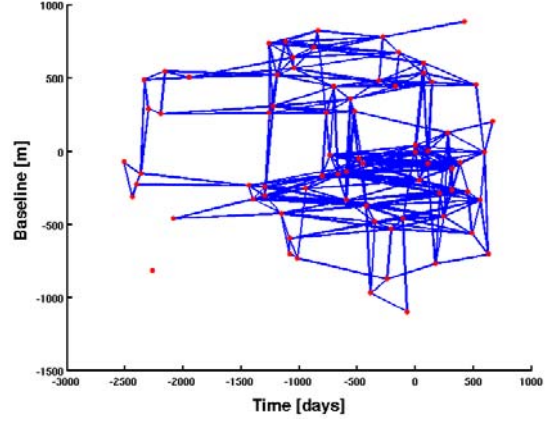


Figure 4. Images graph adopted using baseline limitations.

If it's not request to assure the graph connection, necessary for the unwrapping procedure, we can choose the set of interferograms according to the parameter we want to estimate (height or displacement). For example, if we need height information we can use interferograms with small  $Bt$  (e.g.  $<105$ days), in order to avoid problems due to temporal decorrelation; moreover, as distributed scatters are afflicted by geometrical decorrelation, we can consider interferograms with  $Bn$  less than, say, 700m. In this way we reach a good compromise between interferograms with a suitable lever arm for the desired parameter estimation and those with a good coherence. Dually, for the displacement estimation, we can use e.g.  $Bt < 1000$ days and  $Bn < 150$ m. If we need both the information we can simply combine the two packages of selected interferograms. Fig. 4 shows the obtained graph in the Gardanne data-set.

Regardless of the selected graph, the set of coherent interferograms that carry information can be different from point to point. Again, only PS's are coherent in all interferograms. Thus, in order to estimate height and deformation trend also of partially coherent targets, we have to choose a sub-set of coherent interferograms for each point. To this purpose we can exploit the absolute value of the spatial coherence  $\gamma_p^{i,j}$  of point  $p$ . By inserting it as a weight in the estimation process, only coherent interferograms will determine the result. Eq. 4 becomes then:

$$\xi_p = \frac{\sum_{(i,j)} |\gamma_p^{i,j}| e^{j(\Delta\phi_p^{i,j} - \Delta\bar{\phi}_{H,p}^{i,j} - \Delta\bar{\phi}_{D,p}^{i,j})}}{\sum_{(i,j)} |\gamma_p^{i,j}|} \quad (6)$$

where the denominator has been modified to normalize the outcome. We define as temporal coherence

$\max(|\xi_p|)$ , which can be used as reliability index of the estimation.

Fig. 5 brings a graphical representation of the concept with two examples. The three pictures show the phase residuals (after compensating for the geometrical and the movement terms) of a given point as a function respectively of the spatial coherence (top), the normal (centre) and the temporal (bottom) baselines. The red dots are the phase residuals in the interferograms with spatial coherence  $>0.4$ . What is clearly recognizable from Fig. 5 is that assigning a weight to the phase values allows to identify the information and to discard the noise (the dispersion of the phase values decreases with the coherence). From the distribution of red dots as a function of the normal and temporal baselines it can also be noted that the two selected examples are affected more by temporal than by geometrical decorrelation (red dots are concentrated in small temporal baselines). This fact can have consequences on the accuracy of the estimate of the deformation trend. The smaller the lever arm, the less accurate is the estimate. In order to evaluate the accuracy, we introduce the index  $Bt_p^{eff}$  for each point  $p$  that quantifies the effective set of temporal baselines used in the estimate:

$$Bt_p^{eff} = \frac{\sum_{(i,j)} |\gamma_p^{i,j}| \cdot |Bt^{i,j}|}{\sum_{(i,j)} |\gamma_p^{i,j}|} \quad (7)$$

Eq. 7 is the average temporal baseline, weighted by the absolute value of the spatial coherence associated to point  $p$ .

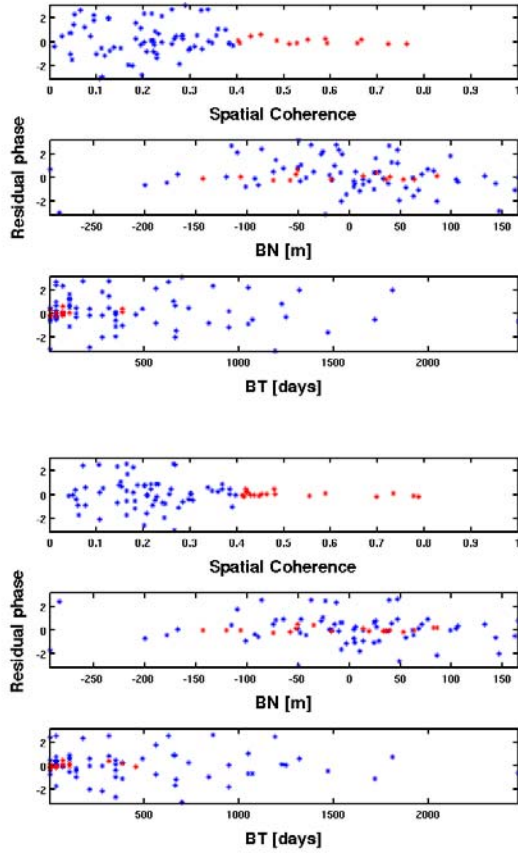


Figure 5. Two examples of residual phase series after removing for the height and deformation trend terms, as a function of spatial coherence (top), normal baseline (centre), temporal coherence (bottom). Red dots: phase samples corresponding to spatial coherence  $> 0.4$ .

The last aspect we take into consideration is the possible extended nature of the target. To this aim we apply a spatial filtering to strengthen the estimate of the interferometric phase associated to the target. Thus we introduce in Eq. 6 the phase of the spatial coherence  $\angle \gamma_p^{i,j}$  instead of the phase of the single pixel:

$$\xi_p = \frac{\sum_{(i,j)} |\gamma_p^{i,j}| e^{j(\angle \gamma_p^{i,j} - \Delta \bar{\phi}_{i,p}^{i,j} - \Delta \bar{\phi}_{D,p}^{i,j})}}{\sum_{(i,j)} |\gamma_p^{i,j}|} \quad (8)$$

Fig. 6 shows two examples (a and b) of phase residuals after compensating for the terms dependent on height and linear deformation trend. In the top images the phase is relative to a single pixel, in the bottom images the phase has been obtained by estimating the spatial coherence. Considering extended targets, the averaging process increases the signal to noise ratio.

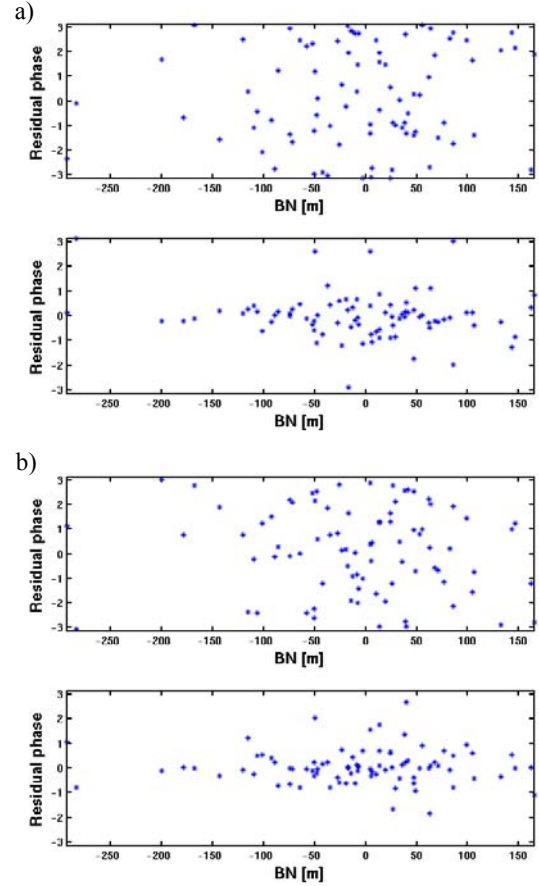


Figure 6. Two examples (a and b) of phase residuals after compensating for the terms dependent on height and linear deformation trend. In the top images the phase is relative to a single pixel, in the bottom ones it has been obtained by estimating the spatial coherence.

### 3. RESULTS

The algorithm above described deals with the core processing step of the PS technique, namely the estimate of height and linear deformation trend of the targets. The algorithm can thus be easily inserted in the processing chain present in literature [2] without remarkable changes. We neglect here describing again the selection of PS Candidates (PSC), the generation of a spatial graph among PSC's and the estimate of the Atmospheric Phase Screen (APS). We introduce hence the analysed data-set and the significant results.

For the analysis of height and velocity field of the region of Dossena we used MST algorithm to choose interferograms and we extracted information only on points considered a priori reliable according to their amplitude stability. The processed area is partially visible as background in Fig. 7 at the top. It corresponds to an area of approximately  $100\text{km}^2$  on the ground. The data have been acquired by the European Space Agency

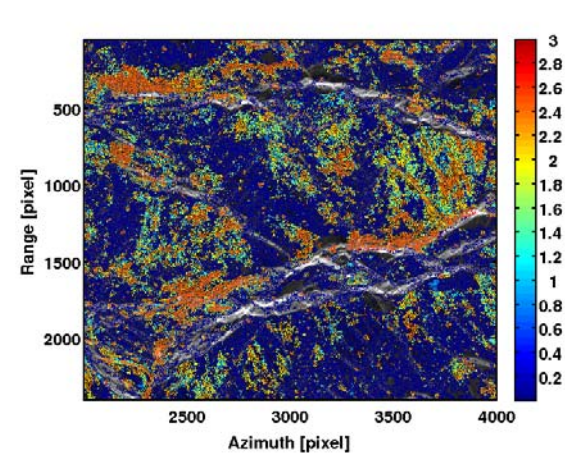
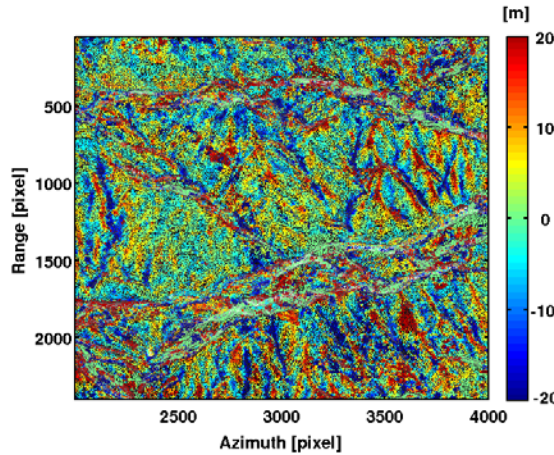
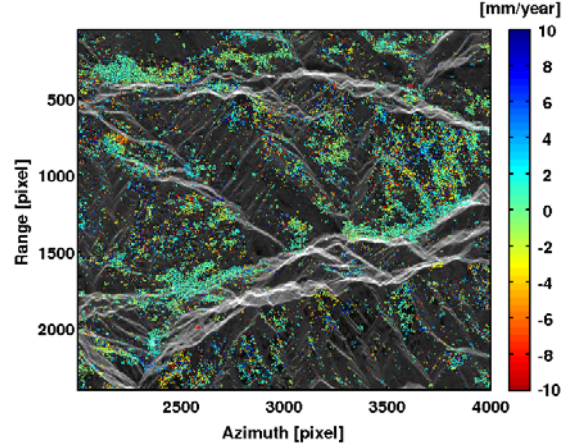
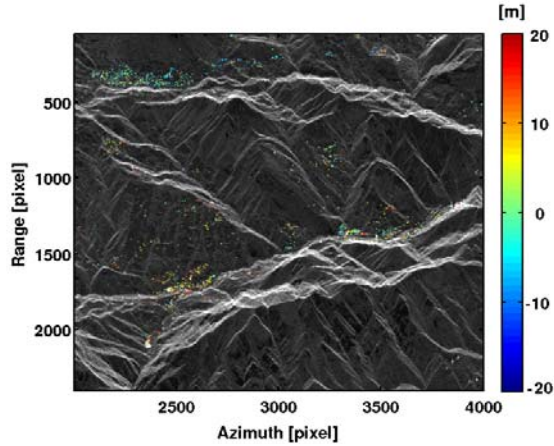


Figure 7. Estimated residual height (with respect to SRTM data) in a colour scale ranging 40m, for classical PS's (top) and for partially coherent targets (bottom).

Figure 8. Velocity of displacement estimated over partially coherent targets (top) and effective temporal baseline (bottom, the colour represents the logarithm in base 10) obtained with the MST.

(ESA) satellites ERS-1 and 2 from the descending Track 208, Frame 2673. The analysed 84 images cover the time-period from 1992 to 2003. Fig. 7 reports the first results. The estimated residual height (with respect to SRTM data) is plotted in a colour scale ranging 40m for the classical PS's (at the top) and for the partially coherent targets detected with the proposed modifications (at the bottom). The two images are actually not fully comparable: the classical PS (~1500 points) have been selected posing a restrictive threshold on the temporal coherence ( $>0.7$ ), whereas at the bottom 160.000 points have been chosen with a temporal coherence  $>0.4$ . It is appreciable the density of points even in vegetated areas and the height details that can be easily recognized. Moreover, it can be observed that most of the topographic features that have become

visible are in correspondence of slope changes. This fact, that deserves future studies, can be at least firstly explained considering that SRTM errors lead not only to wrong height values in SAR coordinates, but to wrong height values also in wrong SAR coordinates. This shift between real and SRTM height data in SAR coordinates produces, when calculating their difference, height steps exactly in correspondence of slope changes.

Fig. 8 shows at the top the results relative to the estimate of the linear deformation trend, while at the bottom it reports the index in Eq. 7 for all the analysed points in a logarithmic scale. This picture can be interpreted as the effective life time of the scatterers. Red identifies permanent scatterers, blue very short living points whose linear deformation trend cannot be accurately estimated.

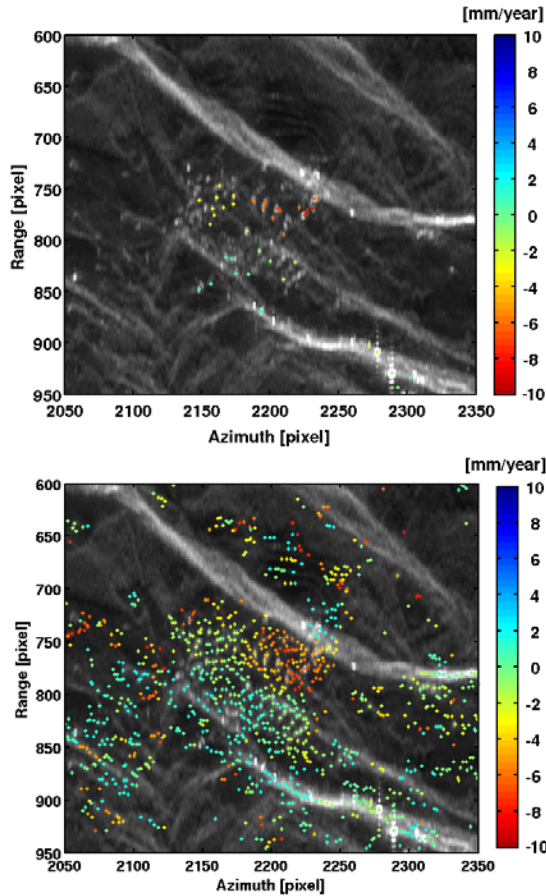


Figure 9. Estimated linear deformation trends of PS's (top) and of partially coherent targets (bottom) around the municipality of Dossena. The orange-red identifies the active landslide.

Finally, in Fig. 9 a comparison over the municipality of Dossena is depicted. At the top the PS and at the bottom the partially coherent targets velocities are shown. The deformation values of the two images are in good agreement. The main contribution of the novel technique resides in the possibility to precisely locate the moving area within the scene. This is the main aim for which geologists decided to commission the deformation analysis to spaceborne radar techniques. If fact, even if the area of Dossena has been classified as a risk zone due to an active landslide on its territory since 1998, the boundary of the risk zone have never been checked with precision.

For the region of Gardanne we used instead the second approach for interferograms selection. We created the connection graph among images imposing limits to temporal and normal baselines in order to reduce decorrelation problems. In this case we analysed all the pixels without an a priori selection.

The processed area is visible as background in Fig. 10 at the top. It corresponds to an area of approximately

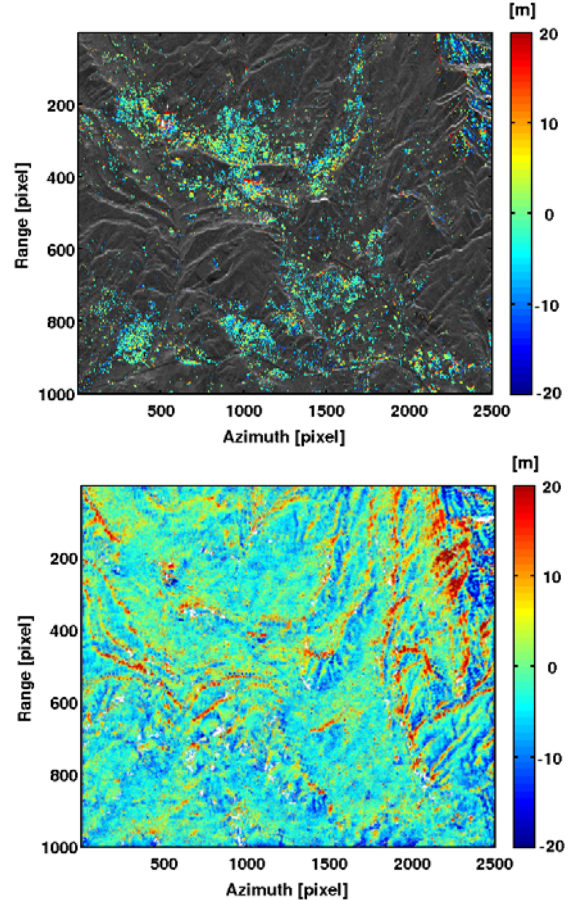


Figure 10. Estimated residual height (with respect to SRTM data) in a colour scale ranging 40m, for classical PS's (top) and for partially coherent targets (bottom).

100km<sup>2</sup> on the ground. The data have been acquired by the European Space Agency (ESA) satellites ERS-1 and 2 from the descending Track 65, Frame 2727. The analysed 74 images cover the time-period from 1992 to 2001.

The estimated residual height (with respect to SRTM data) is plotted in a colour scale ranging 40m for the classical PS's (at the top) and for the partially coherent targets (at the bottom). With the classical PS technique we find the 2.5% of coherent points, whereas with the new algorithm we estimate the height nearly over all pixels, even if with lower accuracy.

Fig. 11 shows the results relative to the estimate of the linear deformation trend.

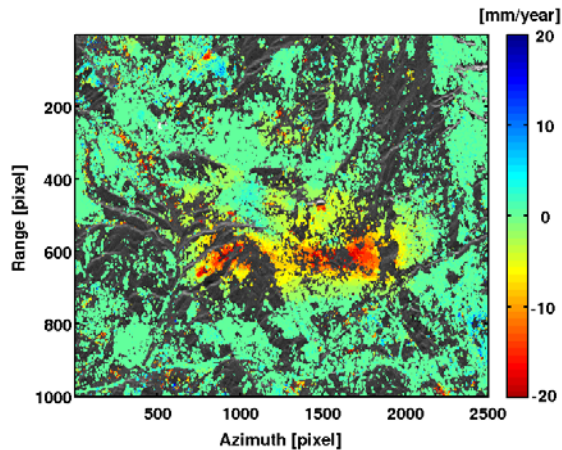


Figure 11. Velocity of displacement estimated over partially coherent targets.

Also in this case we have a lower density of measure points for the velocity field respect to the elevation one, because temporal decorrelation has a stronger effect than geometrical decorrelation. What we see in Fig. 11 is the estimated velocity field that represents the linear regression of the deformation trend in Gardanne, which is known being affected by non-linear motions [10].

#### 4. CONCLUSIONS

In this work we developed a new processing algorithm that allows extracting information also from partially coherent targets using spaceborne SAR data. Thus, very high densities of points can be reached also in extrurban areas to monitor surface linear deformation phenomena (with about 10 times more coverage with respect to PSs) and to retrieve Digital Elevation Maps (100 times more w.r.t. PSs).

#### 5. ACKNOWLEDGEMENTS

The authors are very thankful to TRE for producing the focused and coregistered data-sets and to Dr GianMarco Orlandi (Studio Associato di Geologia Spada) for giving the possibility of analysing the case study of Dossena.

#### 6. REFERENCES

1. Curlander, J. C. & McDonough, R. N. (1991). *Synthetic Aperture Radar: Systems and Signal Processing*, New York, John Wiley & Sons.
2. Ferretti, A., Prati, C. & Rocca, F. (2001). *Permanent Scatterers in SAR Interferometry*, IEEE TGARS, Vol. 39, no. 1.
3. Dixon, T.H., Amelung, F., Ferretti, A., Novali, F., Rocca, F., Dokkas, R., Sella, G., Kim, S.W., Wdowinski, S. & Whitman, D. (2006). *Subsidence and flooding in New Orleans*, Nature, vol. 441, pp. 587-588.

4. Ferretti, A., Perissin, D., Prati, C. & Rocca, F. (2006). *On the physical characterization of SAR Permanent Scatterers in urban areas*, Proceedings of 6th European Conference on Synthetic Aperture Radar - EUSAR, Dresden (Germany).
5. Ferretti, A., Parizzi, A., Perissin, D., Prati, C. & Rocca, F. (2006). *Accurate DEM reconstruction from Permanent Scatterers and multi-baseline interferometry*, Proceedings of the IEEE International Geoscience and Remote Sensing Symposium - IGARSS, Denver (Colorado).
6. Savio, G., Ferretti, A., Novali, F., Musazzi, S., Prati, C. & Rocca, F. (2005). *PSInSAR Validation by means of a Blind Experiment Using Dihedral Reflectors*, proceedings of FRINGE, Frascati, Italia.
7. Berardino, P., Fornaro, G., Lanari, R. & Sansosti, E. (2002). *A New Algorithm for Surface Deformation Monitoring based on Small Baseline Differential SAR interferograms*, IEEE TGARS, vol. 40, no. 11, pp. 2375-2383.
8. Hooper, A., H. Zebker, P. Segall, and B. Kampes (2004), A new method for measuring deformation on volcanoes and other natural terrains using InSAR persistent scatterers, Geophys. Res. Lett., 31.
9. Refice A., Convenga F., Nutricato R., (2003) *Stepwise approach to InSAR processing of multitemporal datasets*, Proc. of Fringe 2003.
10. Raucoules, D., Bourguin, B., de Michele, M., Le Cozant, G., Closset, L., Bremmer, C., Veldkamp, H., Tragheim, D., Bateson, L., Crosetto, M. & Agudo, M. (2007). *Persistent Scatterers Interferometry Independent Validation and Intercomparison of Results – Final Report*, BRGM/RP-55649-FR.